

Ignition Probability of Lean Premixed Bluff-Body Flames

S. F. Ahmed¹ and E. Mastorakos²

1. Mechanical Engineering, King Fahd University of Petroleum and Minerals, Saudi Arabia.
2. Department of Engineering, University of Cambridge, Cambridge CB2 1PZ, UK.

1 Introduction

Lean combustion is currently employed in nearly all combustion technology fields, including gas turbines; internal combustion engines (ICEs), boilers and furnaces in order to achieve very low emissions and very high efficiency. Interest in lean premixed flames as an attractive alternative for practical combustion systems began in the early 1980s [1]. Currently, major gas turbine manufacturers (e.g., Siemens and GE) are placing emissions and efficiency at the frontline of their research and development. However, for aviation gas turbines in particular, moving towards very lean combustion is restricted by two main difficulties; lean stability (blow-off) and altitude relight (ignitability). Great attention has been given to the stability of lean premixed flames and the problems associated with this issue if operating close to the extinction limit [2,3]. However, the altitude relight or the ignitability of the combustor under this condition has not been studied extensively yet. In general, ignition of turbulent premixed flames has been well characterized and quantified in terms of minimum ignition energy (MIE) and flame propagation speed in a flowing mixture [4-6]. However, studying the ignitability of very lean premixed flames in a complex flow pattern such as a turbulent bluff-body flow, which is similar to the real gas turbine combustor flow pattern, has not been considered yet.

The term "ignition probability" (P_{ign}) has been first introduced in the pioneering work of Birch et al [7] and Smith et al [8]. They have successfully correlated the probability of ignition (defined as just initiation of a flame kernel whether it results in a stable flame or not) in a non-premixed turbulent jet with the probability of finding a flammable mixture at the spark location. Recently, a series of experiments [9-12] and simulations [13-16], driven by the altitude relight problem of the aviation gas turbine, have investigated the ignition probability (defined as a fully establishment of a stable flame) in different turbulent non-premixed and spray flames. In these studies, the successful ignition (practically) includes not only an initiation of a flame kernel, but also flame propagation and overall stability of the flame. This aspect of ignition has been denoted as "phase 2" of a gas turbine ignition process [17]. The above studies have concluded that the failed ignition can happen because of two main reasons; first, failure of the spark to initiate a flame kernel and second, if the flame kernel is initiated, failure of the kernel to propagate and form the stable flame. Both reasons result in reducing P_{ign} [18].

The first reason is associated with local and non-local effects at the spark location. The local effects include: mixture fraction fluctuations [11], velocity fluctuations [9], strain rate [10,13], turbulence [11] and droplet SMD for sprays [12]. On the other hand, the non-local effect can be attributed to the diffusion of the spark energy from the spark location to another location probably due to the influence of the global flow field [10,11]. The second reason of the failure of flame kernel propagation has been found to be linked to the mean mixture fraction, mean flow velocity and mean turbulence ahead of the flame kernel [9-11]. If all these parameters are favorable for upstream flame propagation, the flame kernel will propagate and establish the stable flame. In this case, the ignition can be described as successful. Due to all these parameters, operating with very lean turbulent premixed flames is expected to be a challenging task regards the ignitability of the engine. Therefore, investigating P_{ign} of such flames in a flow field relevant to a real combustor is important in order to provide the engine manufacturers information on the ignition capability.

2 Experimental methods

2.1 Apparatus

The burner used in the present work, Fig. 1, consists of two concentric circular ducts of length 400 mm. The inner diameter of the outer duct, D_s , is 35 mm. The inner duct is a 6-mm-internal diameter tube of wall thickness 0.5 mm and its end at the burner exit has a conical bluff body of diameter $D_b = 25$ mm, giving a blockage ratio $BR = D_b^2/D_s^2 = 50\%$. The flame area was enclosed using an 80-mm-long fused silica quartz cylinder of inner diameter 70 mm, which provided optical access for the imaging and also avoided air entrainment from the surroundings. More details about the design of the burner can be found in Ref. [19]. This burner with exactly the same dimensions has been used before for flame stability and ignition investigations [11,19]. The axial and radial mean and rms velocity fluctuations have been measured using LDV. More details about the flow measurements can be found in Ref. [11]. In general, the flow field consists of a central recirculation zone (CRZ) formed in the wake of the bluff-body and a so-called side recirculation zone (SRZ) formed by the rearward-facing step (dump plane), Fig. 1. The width and the length of the CRZ are about $1 D_b$ and $1.2 D_b$ (D_b is the bluff-body diameter), respectively. Previous measurements have also showed that the turbulence is relatively uniform within the CRZ and peaks above the edge of the bluff-body and is relatively high within the SRZ [11].

Methane (99.96% purity) was used as a fuel. The air and methane were mixed together 2 m upstream of the burner exit, to ensure fully mixing, and the mixture passed through the annulus between the outer and inner ducts, Fig.1. Both air and fuel flow rates were controlled by BRONKHORST HI-Tech mass flow controllers with an accuracy of 0.5% of full scale deflection. The exit velocity of the mixture U was chosen to create highly turbulent flow up to 20 m/s ($Re = 3.34 \times 10^4$ based on D_b) with very lean global equivalence ratios ϕ from 0.5 to 0.7. The flammability limits of this fuel in air are $\phi_{lean} = 0.5$ and $\phi_{rich} = 1.5$ [4]. Figure 1 also shows the flow field patterns of this burner based on previous LDV measurements for the same burner [11].

An inductive ignition system was specially designed to produce repeatable sparks whose energy and duration could be varied independently. Full description and the characteristics of the ignition system are mentioned elsewhere [9]. The spark was created between two tungsten electrodes with diameter 1 mm, which were placed as shown in Fig. 1 to ensure minimum disturbance to the flow. The spark gap width was set to be 2 mm for all experiments. The ignition probability was measured by applying 50 single sparks at each location of interest. The number of successful events that resulted in a stable flame was divided by 50 to calculate the ignition probability, which implies an uncertainty of 7.5% at 50% ignition probability [8]. Under all conditions studied here, the spark had energy of 200 mJ and duration of 500 μ s. The estimated energy transfer efficiency from the spark to the mixture for the current igniter configuration is about 30% [9]. This energy is much higher than the minimum ignition energy (6.41 mJ) required for igniting methane–air mixtures within the flammability limits under atmospheric conditions [20]. Each of the ignition probability contours measured here was assembled from a matrix of 25×25 points across and along the burner.

2.2 High-speed imaging

Different successful and failed ignition events were visualized using a Phantom V4.2 digital high speed camera. Many movies were recorded for such purposes at 4200 fps and an exposure time of 238 μ s with a maximum image size of 512×512 pixel to visualize a region of 80×80 mm of the flow field.

3 Results and discussion

3.1 Flame stability and visualization

The lean extinction velocity of the premixed methane-air bluff-body flames has been studied first to identify the lean stability limit of the burner. Figure 2 shows the extinction exit velocity U_{ex} for different equivalence ratios. For every mixture velocity, the flame has been ignited well above the lean limit. Then, the amount of fuel in the mixture has been reduced slowly and gradually with enough time gap between steps, to allow for the uniformity of the mixture to restore, until the flame disappears. The equivalence ratio at which the flame extinguished was then recorded. This procedure has been repeated many times for each mixture velocity to ensure the consistency of the results. Figure 2 indicates the area where the flame can be established and that where extinction happened.

It can be observed that U_{ex} increases almost linearly with the increase in the equivalence ratio within the current range of interest ($0.5 < \phi < 0.7$). This extinction is mainly due to the high strain rates that the flame experiences before extinction and due to the reduction in the local turbulent flame speed relative to the local flow velocity [21]. This behavior is considered a well-established characteristic of the premixed flame extinction curves for different flame holder geometries [1]. Based on the curve shown in Fig. 2, two flow conditions have been selected for ignition investigation. Condition A ($U = 10$ m/s, $\phi = 0.65$) is well above the extinction curve and condition B ($U = 15$ m/s, $\phi = 0.65$) is very close to extinction, Fig. 2.

Before discussing any further details of the ignition characteristics of this type of flames, visualization of the ignition behavior at different locations within the flow field will be presented. Many ignition events from the moment of spark discharge to the possible stabilization of the flame have been visualized by the high-speed camera. The behavior of the flame propagation after the ignition depends mainly on the ignition location relative to the recirculation zones. Similar behavior has been observed in non-premixed bluff-body flame ignition [11]. Figure 3 shows high-speed camera images of a successful ignition event inside the CRZ at z (axial location above the bluff-body surface) = 40 mm, r (radial location from the bluff-body centerline) = 0 for case B, the one close to extinction. It can be noted that the flame propagates toward the bluff body first, as a response to the negative axial velocity at this location, and then starts propagating from the bluff body downstream until the whole flame within CRZ lights-up. It takes about 10 ms for the flame to be established, much faster than the non-premixed flames ignited at similar locations (about 50 ms) [11]. Once that happens, a separate flame front starts propagating inside the side recirculation zone (SRZ) until the whole enclosure lights-up with the flame at about 14 ms after the spark, Fig. 3. However, soon after that, the flame inside SRZ quenches and then the flame takes its final shape at about 36 ms after the spark, Fig. 3. It is not clear here why this quenching happened in SRZ, but it can be related to the high velocity fluctuations at this location [11], which can lead to quench the turbulent premixed flame propagation at the current $\phi = 0.65$ [22]. This behavior of the flame inside the SRZ has also been observed when the flame was ignited at the same location of condition A. However, it has not been observed in the non-premixed ignition, probably due to the fact that the mixture inside the SRZ is not flammable in this case [11].

Figure 4 shows high-speed camera images of a successful ignition event at $z = 40$ mm, $r = 20$ mm for case B. The flame was ignited outside the CRZ, which resulted in axial flame propagation at the beginning to light up that side of the flow first, and then the flame propagated toward the other side in order to establish the flame. It takes about 11 ms, on average, for the flame to be established from this ignition location. This flame propagation behavior can be understood from the previous velocity measurements of this burner [11]. The mean axial velocity in the location of ignition is much higher than the radial velocity. Therefore, it is expected that the flame propagates in the axial direction first before it propagates radially and tangentially to the other side of the burner. Similar behavior has been observed in the non-premixed flame ignition [11]. This shows that the flow velocity in a complex flow pattern like the current one is the main driver for the direction of the flame propagation regardless the mixture strength or distribution. Similar to the previous ignition location ($z = 40$ mm, $r = 0$ mm), the flame propagates to light-up the SRZ after lighting-up the CRZ. Again, after about 36 ms from the

spark, the flame inside SRZ quenches and the flame forms its final shape as shown in Fig. 4. It should be mentioned that there is absolutely no difference in the flame propagation behavior if a flame of condition *A* has been ignited at the same location.

Although a fully premixed flame has been considered in the present work with $\phi = 0.65$ (within the flammable region), failed ignition events have been observed in some locations within the flow field. This could happen if the flow condition is close to the extinction condition of this flame, similar to case *B*. Figure 5 shows a failed ignition event at $z = 20$ mm, $r = 20$ mm for case *B* (inside the SRZ). It can be seen that there is a beginning of flame kernel initiation as the spark starts. However, the kernel completely disappears once the spark ends, which has been classified before as the first type of failed ignition [11]. It should be mentioned that no other types of failed ignition has been observed in this flow. Once a flame kernel propagates away from the spark location, a successful ignition can be achieved. This indicates that there is a probabilistic nature of ignition of the fully premixed bluff-body flames close to extinction. Igniting the flame at the same location of condition *A* (away from extinction) results always in a successful ignition event. In the next section, the ignition probability of both flow conditions (*A* and *B*) will be presented and discussed.

3.2 Ignition probability

Figure 6a shows the ignition probability of the flame of case *A* ($U = 10$ m/s, $\phi = 0.65$). The ignition probability is 100% everywhere within the enclosure length (80 mm above the bluff-body). This indicates that the available spark energy and duration are adequate to ignite the flame in such configuration. Therefore, any failed ignition in the other case (*B*) is due to the effect of local fluid mechanics conditions on the growth and the propagation of the flame kernel. Above the enclosure, air is entrained and hence the equivalence ratio decreases. Therefore, a consistent reduction in the ignition probability can be observed up to $z = 130$ mm.

Figure 6b shows the ignition probability of the flame of condition *B* ($U = 15$ m/s, $\phi = 0.65$). It can be observed that regions of different ignition probabilities have been created around the CRZ. Above $z = 45$ mm (almost the height of the CRZ), the ignition probability is 100% everywhere and continues similar to condition *A*. The highest ignition probability below $z = 45$ is located at the middle of the CRZ with about 85%. As we move horizontally parallel to the bluff-body surface, the ignition probability decreases gradually until it reaches 0% at about $r = 15$ mm, Fig. 6b. This behavior is consistent with the turbulent intensity profile across the flow field. The turbulence increases gradually from the center of the CRZ at $r = 0$ to the center of the SRZ at $r = 23$ [11]. Previous studies show that, for the flow with uniform turbulence intensity profile (counter-flow for instance), the strain rate is the main parameter that can cause reduction in the ignitability [10,13]. Moreover, it was not possible to ignite such flow if the value of the strain rate is about 90% of the extinction strain rate [10]. However, in a complex flow field such as the present one with non-uniform turbulence intensity and strain rate profiles, the increase in turbulence in some locations is expected to play an important role in quenching the flame kernel at the spark location before it grows and propagates away from the spark. From the present results, the effect of turbulence becomes dominant when the flow condition (U and ϕ) is close to the extinction limit of the flame. This explanation also agrees with the previous investigations of the effect of turbulence on the quenching of turbulent premixed flame propagation [22]. Therefore, the area with the highest turbulence intensity like the SRZ is expected to be the area with the lowest ignition probability and vice versa. This indicates that in order to run a gas turbine with lean premixed flames close to extinction, the re-design of the ignition system is absolutely necessary to achieve high ignitability of the engine.

4 Conclusions

Turbulent lean premixed bluff-body flame ignition has been studied in terms of flame extinction, ignition visualization and ignition probability. Extinction of this flame follows the standard characteristics of premixed flames as U_{ex} increases with the increase of equivalence ratio. High speed

camera images show that the behavior of the flame propagation after the ignition depends mainly on the ignition location relative to the recirculation zones similar to the non-premixed bluff-body flames. Moreover, the flame inside SRZ quenches soon after the whole flame lights-up. Failed ignition has been viewed close to the extinction flow conditions of the flame. Igniting the flame away from the extinction conditions results in 100% ignition probability regardless of the ignition location. However, close to extinction, ignition probability decreases gradually as we move away from the center of the burner and achieving ignition is not possible at all outside the CRZ.

Acknowledgments

This work has been partly funded by the Department of Trade and Industry and Rolls-Royce plc. Thanks to Dr. R. Balachandran from UCL for assistance with the experimental techniques. Samer F. Ahmed wishes to thank King Fahd University of Petroleum and Minerals for the support.

References

- [1] D. Dunn-Rankin, *Lean combustion technology and control* (2008), Academic Press, Burlington,
- [2] D. Bradley, P.H. Gaskell, X.J. Gu, M. Lawes, M.J. Scott (1998), Premixed turbulent flame instability and NO formation in a lean-burn swirl burner, *Combust. Flame* 115, 515–538.
- [3] S.R.N. De Zilwa, J.H. Uhm, J.H. Whitelaw (2000), Combustion oscillations close to the lean flammability limit. *Combust. Sci. Technol.* 161, 231–258.
- [4] D.R. Ballal, A.H. Lefebvre (1976), The influence of flow parameters on minimum ignition energy and quenching distance, *Proc. Combust. Inst.* 15, 1473–1481.
- [5] D.R. Ballal, A.H. Lefebvre (1980), A general model of spark ignition for gaseous and liquid fuel-air mixtures, *Proc. Combust. Inst.* 18, 1737–1746.
- [6] C.F. Kaminski, J. Hult, M. Alden, S. Lindenmaier, A. Dreizler, U. Mass, M. Baum (2000), Spark ignition of turbulent methane air mixtures revealed by time-resolved planar laser-induced fluorescence and direct numerical simulations, *Proc. Combust. Inst.* 28, 399–405.
- [7] A.D. Birch, D.R. Brown, M.G. Dodson (1981), Ignition probabilities in turbulent mixing flows, *Proc. Combust. Inst.* 18, 1755–1780.
- [8] M.T.E. Smith, A.D. Birch, D.R. Brown, M. Fairweather (1986), Studies of ignition and flame propagation in turbulent jets of natural gas, propane and a gas with a high hydrogen content, *Proc. Combust. Inst.* 21, 1403–1408.
- [9] S.F. Ahmed, E. Mastorakos (2006), Spark ignition of turbulent lifted jet flames, *Combust. Flame* 146, 215–231.
- [10] S.F. Ahmed, R. Balachandran, E. Mastorakos (2007), Measurements of ignition probability in turbulent non-premixed counterflow flames, *Proc. Combust. Inst.* 31, 1507–1513.
- [11] S.F. Ahmed, R. Balachandran, T. Marchione, E. Mastorakos (2007), Spark ignition of turbulent non-premixed bluff-body flames, *Combust. Flame* 151, 366–385.
- [12] T. Marchione, S.F. Ahmed, E. Mastorakos (2009), Ignition of turbulent swirling n-heptane spray flames using single and multiple sparks, *Combust. Flame* 156, 166–180.
- [13] E. Richardson, E. Mastorakos (2007), Numerical investigation of spark-ignition in a laminar methane-air counterflow, *Combust. Sci. and Tech.* 179, 21–37.
- [14] N. Chakraborty, E. Mastorakos (2006), Numerical investigation of edge flame propagation characteristics in turbulent mixing layers, *Phys. Fluids* 18, 105103.

- [15] N. Chakraborty, E. Mastorakos, R.S. Cant (2007), Effects of turbulence on spark ignition in inhomogeneous mixtures: a direct numerical simulation (DNS) study, *Combust. Sci. Technol.* 179, 293–317.
- [16] N. Chakraborty, E. Mastorakos (2008), Direct numerical simulations of localised forced ignition in turbulent mixing layers: the effects of mixture fraction and its gradients, *Flow Turbulence Combust.* 80, 155–186.
- [17] A.H. Lefebvre (1998), *Gas Turbine Combustion*, Taylor and Francis, London.
- [18] E. Mastorakos (2009), Ignition of turbulent non-premixed flames. *Prog. Energy Combust. Sci.*, 35, 57.
- [19] R. Balachandran, B.O. Ayoola, C.F. Kaminski, A.P. Dowling (2005), E. Mastorakos, Experimental investigation of the nonlinear response of turbulent premixed flames to imposed inlet velocity oscillations, *Combust. Flame* 143, 37–55.
- [20] B. Lewis, G.V. Elbe (1987), *Combustion, Flames and Explosions of Gases*, Harcourt Brace Jovanovich, London.
- [21] E. Korusoy, J.H. Whitelaw (2004), Effects of wall temperature and fuel on flammability, stability and control of ducted premixed flames, *Combust. Sci. and Tech.* 176, 1217-1241.
- [22] R.G. Abdel-Gayed, D. Bradley, F.K.-K. Lung (1989), Combustion regimes and the straining of turbulent premixed flames, *Combust. Flame* 76, 213–218.

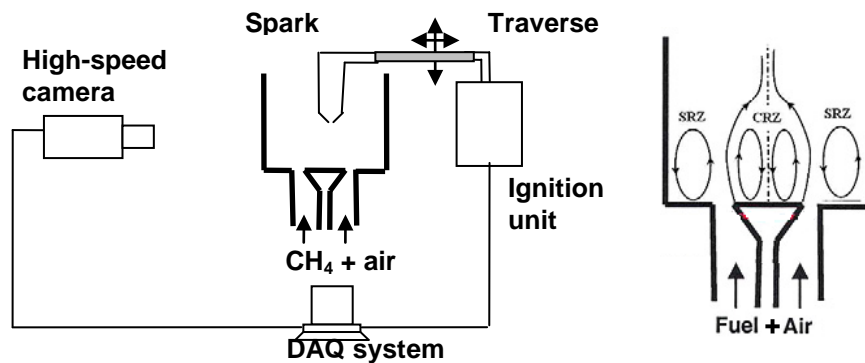


Fig. 1. Schematic of the test rig and flow patterns.

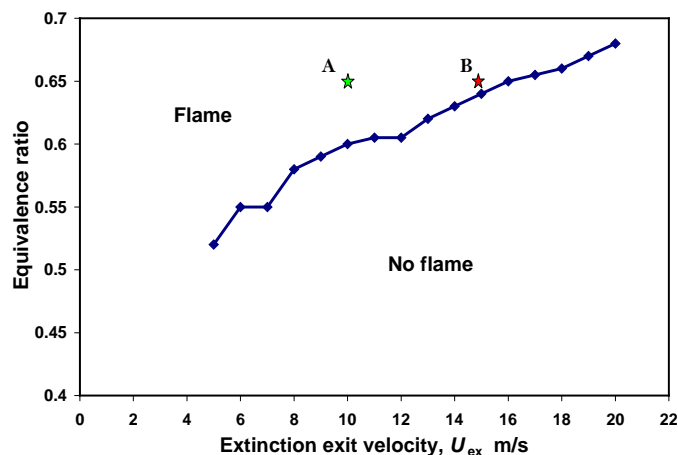


Fig. 2. Lean extinction exit velocity as a function of equivalence ratio.

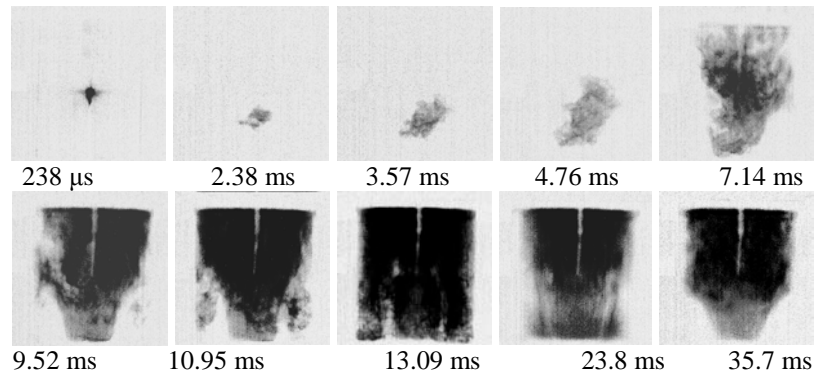


Fig.3. Instantaneous high-speed camera images of an ignition event of case B ($U = 15$ m/s, $\varnothing = 0.65$) with 4200 fps and exposure time $238 \mu\text{s}$. Ignition at $z = 40$ mm, $r = 0$ mm. The images cover a region of 80×80 mm.

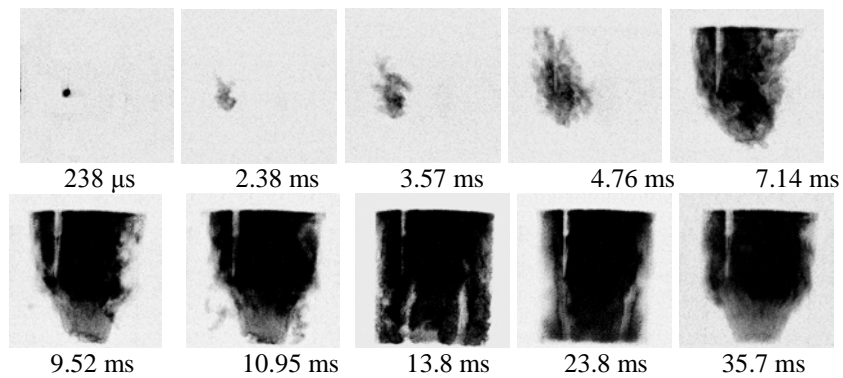


Fig.4. Instantaneous high-speed camera images of an ignition event of case B with 4200 fps and exposure time $238 \mu\text{s}$. Ignition at $z = 40$ mm, $r = 20$ mm. The images cover a region of 80×80 mm.

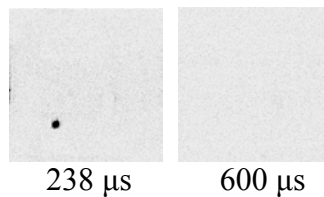


Fig.5. Instantaneous high-speed camera images of a failed ignition event of case B with 4200 fps and exposure time $238 \mu\text{s}$. Ignition at $z = 20$ mm, $r = 20$ mm. The images cover a region of 80×80 mm.

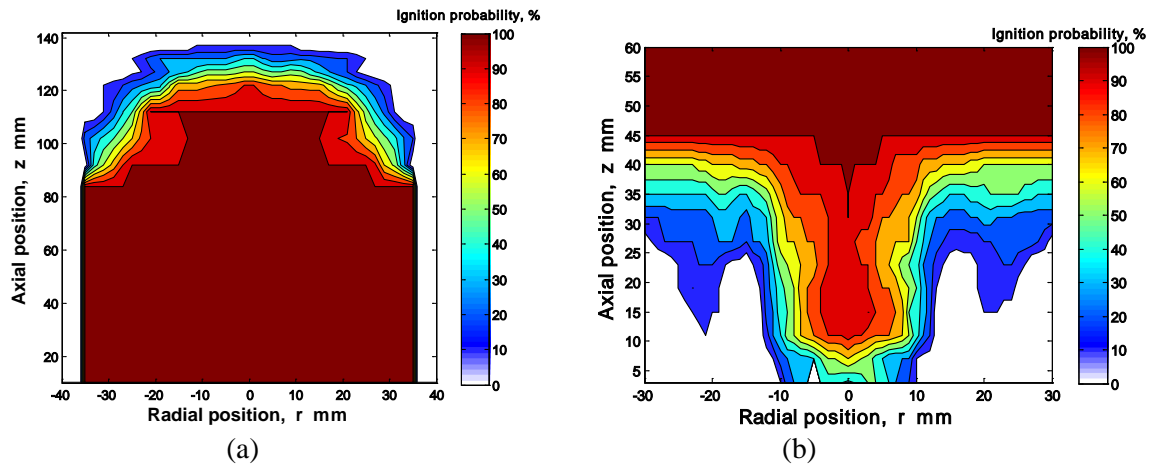


Fig.6. Ignition probability contour of (a) case A, $U = 10$ m/s, $\text{Ø} = 0.65$. (b) case B, $U = 15$ m/s, $\text{Ø} = 0.65$. Spark for both cases: 200 mJ and 500 μ s.